

# Comparing Methods of Characterizing Energetic Disorder in Organic Solar Cells

Paula Hartnagel, Sandheep Ravishankar, Benjamin Klingebiel, Oliver Thimm, and Thomas Kirchartz\*

The energetic disorder has been known for decades to limit the performance of structurally disordered semiconductors such as amorphous silicon and organic semiconductors. However, in the past years, high-performance organic solar cells have emerged showing a continuously reduced amount of energetic disorder. While searching for future high-efficiency material systems, it is therefore important to correctly characterize this energetic disorder. While there are several techniques in the literature, the most common approaches to probe the density of defect states are using optical excitation as in external quantum efficiency measurements, or sequential filling of the tail states by applying an external voltage as in admittance spectroscopy. A metanalysis of available literature, as well as the experiments using four characterization techniques on two material systems, reveal that electrical, voltage-dependent measurements frequently yield higher values of energetic disorder than optical measurements. With drift-diffusion simulations, it is demonstrated that the approaches probe different energy ranges of the subband-gap density of states. The limitations of the techniques are further explored and it is found that extraction of information from a capacitance-voltage curve can be inhibited by internal series resistance. Thereby, the discrepancies between measurement techniques with sensitivity to different energy ranges and electronic parameters are explained.

10% mark.<sup>[1–3]</sup> The substantially reduced performance of, for example, amorphous silicon relative to crystalline silicon is to a major degree caused by increased charge trapping and recombination due to energetic disorder evoked by the structural disorder of the amorphous materials.<sup>[4–6]</sup> In the world of organic semiconductors, the disorder has also been frequently considered to be a major obstacle to reaching higher efficiencies.<sup>[7–9]</sup> For a long time during the development of organic photovoltaics, efficiencies were struggling to reach 10% leading to a seemingly similar situation as with amorphous silicon solar cells.<sup>[10]</sup> Over the last several years, however, new polymers and especially new acceptor molecules have completely changed the situation. By now, organic solar cell efficiencies exceed 19% in single-junction devices<sup>[11–15]</sup> and 20% for tandem organic solar cells,<sup>[16]</sup> thereby reaching efficiencies nearly twice that of typical amorphous silicon solar cells. Thus, while structural and energetic disorder will certainly still be present in current state-of-the-art organic solar cells, either

the degree or the impact of the disorder has to be substantially reduced relative to amorphous silicon. Hence, a closer look at energetic disorder and its impact on device performance for current generations of organic solar cells is needed. To achieve this goal, it is crucial to use sensible parameters to quantify disorder, to use reliable measurement methods, and to be aware of the potential limitations of the methods.


While for inorganic semiconductors, the energetic disorder causes shallow trap states in the energy gap between continuous bands, for organic solar cells, states at the donor:acceptor interface, such as the charge-transfer states or local excited states, constitute the band gap. Here, energetic disorder as observed, for example, in absorption and emission measurements is explained by two significantly different physical concepts that are usually referred to as static and dynamic disorder. Static disorder originates from a broadened density of states that is caused by a structural disorder of, for example, polymer chains.<sup>[17]</sup> The dynamic disorder is caused by a combination of two effects: the first is the presence of a non-zero reorganization energy, that is, a displacement of the vibrational ground state of the electronically excited state relative to the electronic

## 1. Introduction

Amorphous inorganic semiconductors have been studied over decades for photovoltaic applications but were eventually discarded because of poor performance that hardly exceeded the

P. Hartnagel, S. Ravishankar, B. Klingebiel, O. Thimm, T. Kirchartz  
IEKS-Photovoltaik  
Forschungszentrum Jülich  
52425 Jülich, Germany  
E-mail: t.kirchartz@fz-juelich.de

T. Kirchartz  
Faculty of Engineering and CENIDE  
University of Duisburg-Essen  
Carl-Benz-Str. 199, 47057 Duisburg, Germany

 The ORCID identification number(s) for the author(s) of this article can be found under <https://doi.org/10.1002/aenm.202300329>.

© 2023 The Authors. Advanced Energy Materials published by Wiley-VCH GmbH. This is an open access article under the terms of the Creative Commons Attribution License, which permits use, distribution and reproduction in any medium, provided the original work is properly cited.

DOI: 10.1002/aenm.202300329

ground state. The second factor is the thermal broadening of these states, that is, the existence of vibrationally excited states with a non-zero occupation probability.<sup>[18,19]</sup> The corresponding reorganization energy after absorption or emission is frequently used to characterize disorder by extracting the width of a Gaussian fit to the data.<sup>[19–23]</sup> Alternatively, it is equally common to describe the experimentally observable disorder in absorption and emission spectra using an exponential Urbach tail whose temperature dependence provides some information about the relative importance of static and dynamic disorder.<sup>[21,24]</sup> The debate is ongoing on which effect is dominating, the energetic disorder of the actual density of states or the reorganization energy.<sup>[20,21,23,25]</sup> However, both effects are detrimental to device performance via their impact on charge transport and recombination.<sup>[26–28]</sup> Thus, the experimental quantification of the energetic disorder remains important independent of the exact origin of the disorder. There are several different methods to measure the disorder, the most prominent among them are optical methods where the absorption or emission of a sample is recorded.<sup>[29–35]</sup> These are followed by electrical methods, where the voltage is varied to move the quasi-Fermi levels over the subband-gap density of states and thereby fill or empty the broadened density of states.<sup>[36–39]</sup> Given that observables, such as the current or the capacitance, depend on the carrier density inside a device under certain conditions, measurements, such as charge extraction<sup>[36–38]</sup> or capacitance-voltage,<sup>[39]</sup> have been used to extract information on the band tails.

**Figure 1** shows how band tails impact photovoltaic performance and how typical values of the reported Urbach energies depend on the type of device and the mode of measurement. Figure 1a shows the simulated impact of the width of the Urbach tail on device performance using parameters typical for organic solar cells (see Table S1, Supporting Information). The histogram shown in Figure 1b provides evidence that the development of nonfullerene acceptors (NFAs) has not only improved power conversion efficiencies of organic solar cells but has also generally reduced the reported Urbach energies relative to the formerly predominant fullerene acceptors (FAs). A substantial number of reports of Urbach tails are now close to the thermal energy  $kT$ , which is highly significant for device performance from a theoretical and practical perspective.<sup>[40]</sup> Figure 1c shows a histogram of Urbach energies resolved for the general class of measurement technique. Here, we discriminate between optical techniques, such as photothermal deflection spectroscopy (PDS) or Fourier-transform photocurrent spectroscopy (FTPS), that probe photon absorption and essentially measures the joint density of states and electrical techniques that use changes in applied voltage to scan the energy-dependent density of states. Here, we note that optical techniques very frequently lead to fairly low Urbach energies around  $kT$  or slightly higher, while electrical techniques give values in a very broad range with a significant number of cases going up to  $3kT$ . Thus, Figure 1c suggests that different methods may systematically lead to different Urbach energies, which would stipulate a closer look at the methods themselves. However, the assessment of Figure 1c is insofar incomplete as it provides only statistical evidence for a method-specific difference but does not provide data, where several techniques have been explored on the same samples.

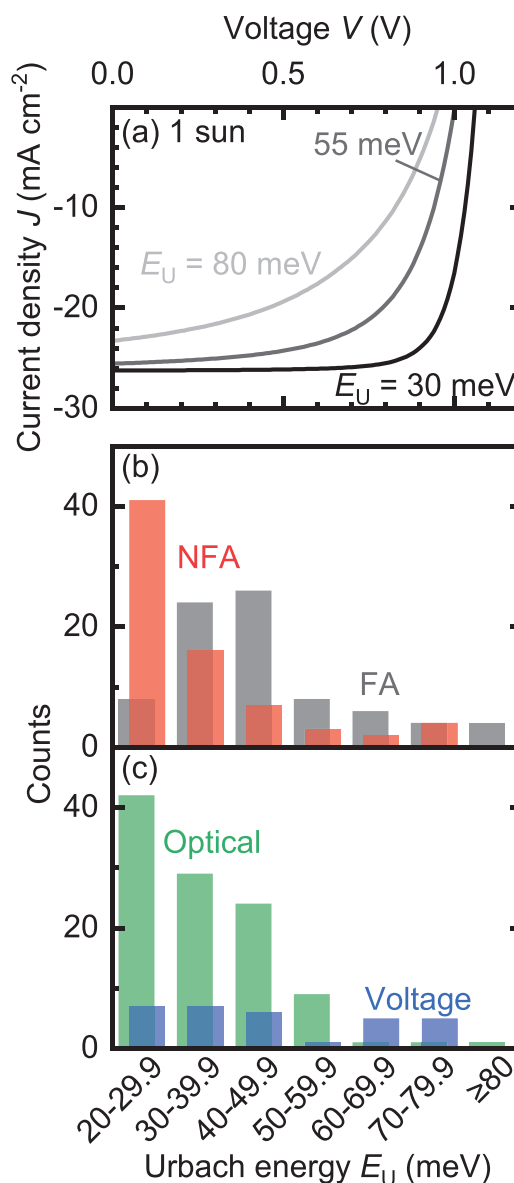


**Figure 1.** a) Simulated current-density voltage curves of organic solar cells with increasing energetic disorder under solar illumination. The performance significantly deteriorates with increasing Urbach energy  $E_U$ . Still, Urbach energies reported in literature differ between b) fullerene (FA)<sup>[7,31,35–37,39,41–72]</sup> and nonfullerene acceptors (NFA)<sup>[29–35,38,39,47–50,73–92]</sup> and especially between c) optical<sup>[7,29–35,41,42,48–62,73–89]</sup> and electrical voltage-dependent<sup>[36–39,45,46,68–71,91,92]</sup> measurement techniques highlighting inconsistencies in the characterization of energetic disorder in organic solar cells. Table S2, Supporting Information, lists all materials, methods, and references from this figure.

Here, we provide such a study of different measurement techniques on the same samples and show how to overcome major issues with the measurement and interpretation of Urbach energies in NFA-based organic solar cells. We compare four different types of measurements done on two different types of organic solar cells. For the optical measurements, we performed PDS on the material films on glass and FTPS on full solar cells. These solar cells, we also characterized with

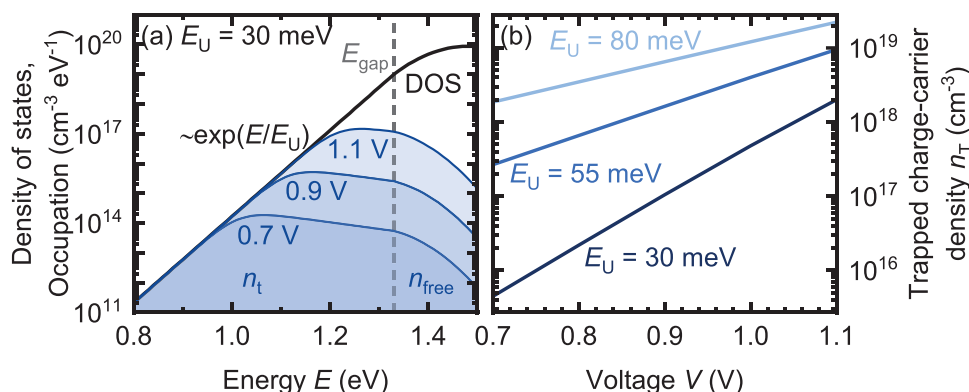


**Figure 2.** a) Modeled density of states around the LUMO of the acceptor with exponential band tails. As the occupation maximum of the density of states is located at the quasi-Fermi level of electrons, the density  $n_T$  of trapped electrons increases with quasi-Fermi level splitting. Consequently,  $n_T$  increases with voltage in b) for Urbach energies  $E_U$  of 30, 55, and 80 meV. Low Urbach energies  $E_U$  result in a more rapid increase since the density of tail states is steeper.

electrical, voltage-dependent methods, where we chose admittance spectroscopy and extracted the Urbach energy from measurements in the dark and at open circuit. We find that Urbach energies indeed vary greatly depending on the methods used. To explain these discrepancies, we more closely investigate artifacts that are arising from capacitance-based measurements. We also highlight the importance of considering the different energy ranges accessed by the different methods. Thereby, we offer insights for a more conclusive characterization of energetic disorder in organic solar cells in the future.

## 2. Extracting the Urbach Energy from Admittance Spectroscopy

In a simplified case, the static disorder in the form of shallow defect states can be modeled by an exponential with the inverse slope  $E_U$ , the Urbach energy,<sup>[93]</sup> as shown in **Figure 2a**. When out of equilibrium, the density of states is occupied according to the Shockley–Read–Hall distribution by charge carriers with an occupancy of  $1/2$  at the quasi-Fermi level of the respective charge-carrier type, which leads to an occupation maximum for an exponential density of tail states. With increasing applied voltage  $V$ , the quasi-Fermi level splitting increases and thereby, more charge carriers occupy the defect states as illustrated in **Figure 2a** for a device in the dark. The resulting density  $n_T$  of trapped charge carriers, therefore, depends on the slope of the density of tail states. This dependence is further illustrated in **Figure 2b** which shows the  $n_T$  as a function of voltage for three different Urbach energies  $E_U$ . The trapped charge-carrier density increases exponentially with voltage with a higher slope for a low Urbach energy since the corresponding density of tail states is steeper. Hence, the voltage dependence of the density of trapped charge carriers  $n_T$  can reflect the shape of the density of states. In a simplified case, this relation can be described by  $n_T \approx \exp(qV/(2E_U))$  (see Section S1, Supporting Information, for the derivation). As can be seen from **Figure 2a**, the area below the band edge that represents  $n_T$  can be significantly larger than the one indicating the free carrier density  $n_{\text{free}}$  in the band, allowing the approximation of the total charge-carrier density  $n = n_T + n_{\text{free}} \approx n_T$ . Hence, to extract the Urbach energy from

electrical measurements, one can try to measure the charge-carrier density as a function of voltage.

Typical methods for finding  $n$  are charge-extraction measurements and capacitance-voltage measurements from admittance spectroscopy. While the first measures the current that is extracted when switching a device from open circuit under illumination to short circuit in the dark, the latter uses the fact that separation of charges is needed to create a capacitance inside a solar cell. A common approximation for this capacitance is

$$C_\mu = qd \frac{dn}{dV} \quad (1)$$

where  $C_\mu$  is the chemical capacitance per area of the charge carriers inside the bulk,<sup>[94,95]</sup> in contrast to the electrode capacitance  $C_\sigma$ . Together, they form the total capacitance  $C = C_\mu + C_\sigma$ .<sup>[96]</sup> Note that here, as well as in charge-extraction measurements, charge-carrier densities are averaged over the active layer thickness. There is no spatial resolution. With this simplification and the previous assumptions on the total carrier density  $n$ , one can write

$$C_\mu \propto \frac{dn}{dV} \propto \frac{dn_T}{dV} \propto \frac{d}{dV} \left( \exp \left[ \frac{qV}{2E_U} \right] \right) \propto \exp \left[ \frac{qV}{2E_U} \right] \quad (2)$$

Hence, from the logarithmic slope of the chemical capacitance  $C_\mu$ , the Urbach energy  $E_U$  can be extracted in this model. In literature, the chemical capacitance most commonly is further integrated to get the charge-carrier density  $n$  and interpret it in terms of recombination mechanisms.<sup>[34,39,96–100]</sup> While the correlation between  $n$  and the recombination rate is relatively intuitive, there are multiple approaches and some discussion on how to proceed with this integration and how to estimate the chemical capacitance.<sup>[96,99,101]</sup> A more detailed analysis of the issues of extracting the Urbach energy from the charge-carrier density can be found in Section S2, Supporting Information. For these reasons, we herein refrain from using further calculation steps during integration and directly use the slope of the chemical capacitance for the Urbach-energy estimation.

To validate this approach and find the most accurate way to calculate the chemical capacitance from admittance data, we modeled a generic organic solar cell using the drift-diffusion

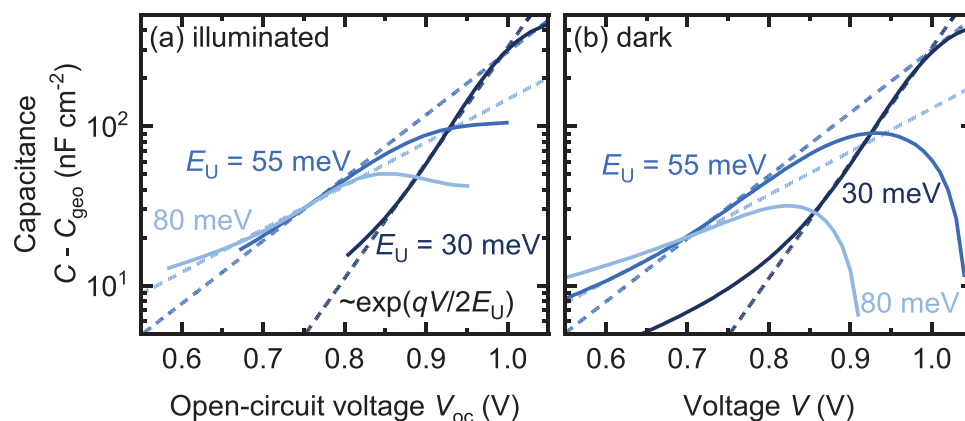


**Figure 3.** Capacitance  $C - C_{\text{geo}}$  extracted from simulated admittance spectroscopy measurements as a function of voltage for Urbach energies  $E_U$  of 30, 55, and 80 meV. The dashed lines indicate an exponential with the corresponding Urbach energy. For both operating conditions, a) under illumination at open circuit and b) in the dark, the quasi-Fermi level splitting can be approximated by the applied voltage and thereby the chemical capacitance can indicate the respective Urbach energy.

simulation software SCAPS.<sup>[102,103]</sup> For simulations under illumination, we further used the software ASA<sup>[104,105]</sup> and optical data from Reference [106] to create the spatially resolved generation rate. Further details on the model and the simulation parameters can be found in Section S3, Supporting Information. Since the extraction of the chemical capacitance from admittance data is not obvious, we first performed simulations to find the best estimation for  $C_\mu$ . These simulations show that the chemical capacitance can be best replicated by subtracting the total capacitance at high frequency and reverse bias in the dark, the geometric capacitance  $C_{\text{geo}}$ , from the total capacitance at low frequencies. Section S4, Supporting Information, describes in more detail how we calculate the chemical capacitance in this work.

Now being able to estimate the chemical capacitance from the simulated admittance data, we test the method of extracting the Urbach energy from the  $C_\mu \propto V$ -relation. For this purpose, **Figure 3** shows the chemical capacitance  $C_\mu$  of three organic solar cells with different tail slopes  $E_U$  of 30, 55, and 80 meV that were calculated from admittance spectroscopy simulations a) under illumination at open circuit and b) in the dark using the approximation  $C_\mu \approx C - C_{\text{geo}}$ . The dashed lines represent the exponential increase that can ideally be expected for the respective Urbach energies. In fact, under both conditions where the quasi-Fermi level splitting can be approximated by the applied voltage, in the dark and at open circuit, the slope of the capacitance  $C - C_{\text{geo}}$  decreases with increasing Urbach energy. This observation shows that the chemical capacitance is sensitive to the shape of the density of defect states and that the Urbach energy extracted from exponential fits can be used as an estimate for the severity of the energetic disorder. However, when applying this method, the frequency of the alternating voltage has to be selected carefully since the charge carriers inside the active layer need to be able to follow the changes in the electric field (see Figure S7, Supporting Information). If the frequency is too high, the capacitance will saturate the geometric capacitance.

This introduction of the rationale behind the characterization of energetic disorder with electrical methods already reveals multiple approximations that go into the analysis and

therefore must be considered when discussing results. On the other hand, while the principle of exciting an electron to or from a trap state by low-energy photons appears more simple, the interpretation of such absorption data remains challenging. The static disorder influencing the shape of the absorption tail can be caused by a disorder in the charge-transfer state, local excitons, or both.<sup>[107]</sup> Additionally, differentiating between static and dynamic disorder has been a topic of discussion in the literature.<sup>[20,21,23,25]</sup> Therefore, we present the following different approaches to interpreting optical data but also discuss electrical and admittance data in detail.

### 3. Experimental Results

To study the difference between optical and voltage-dependent measurements of the Urbach energy  $E_U$ , we characterized two organic solar cells with identical cell architecture but different active layer material systems. More specifically, we used the NFAs (2,2'-(2Z,2'Z)-((12,13-bis(2-butylloctyl)-3,9-diundecyl-12,13-dihydro-[1,2,5]thiadiazolo[3,4-e]thieno[2,3'':4',5']thieno[2',3':4,5]pyrrolo[3,2-g]thieno[2',3':4,5]thieno[3,2-b]indole-2,10-diyl)bis(methanylylidene))bis(5,6-difluoro-3-oxo-2,3-dihydro-1H-indene-2,1-diylidene))dimalononitrile (BTP-4F-12, **Figure 4a**) and (Z)-5-[[5-(15-{(Z)-(3-Ethyl-4-oxo-2-thioxo-1,3-thiazolidin-5-ylidene)methyl]-8thia-7,9-diazabicyclo[4.3.0]nona-1(9),2,4,6-tetraen-2-yl]-9,9,18,18-tetrakis(2-ethylhexyl)-5,14-dithiapentacyclo[10.6.0.0<sup>3,10</sup>.0<sup>4,8</sup>.0<sup>13,17</sup>octadeca-1(12),2,4(8),6,10,13(17),15-heptaen-6-yl)-8-thia-7,9-diazabicyclo[4.3.0]nona-1(9),2,4,6-tetraen-2-yl]methylidene)-3-ethyl-2-thioxo-1,3-thiazolidin-4-one (EH-IDTBR, **Figure 4b**) and the polymer donors Poly[(2,6-(4,8-bis(5-(2-ethylhexyl-3-fluoro)thiophen-2-yl)-benzo[1,2-b:4,5-b']dithiophene))-alt-(5,5-(1',3'-di-2-thienyl-5',7'-bis(2-ethylhexyl)benzo[1',2'-c:4',5'-c']dithiophene-4,8-dione))-ran-poly[(2,6-(4,8-bis(5-(2-ethylhexyl)thiophen-2-yl)-benzo[1,2-b:4,5-b']dithiophene))-alt-(2,2-ethyl-3(or4)-carboxylate-thiophene)] (PBDB-TF-T1, **Figure 4c**) and poly[(5,6-difluoro-2,1,3-benzothiadiazol-4,7-diyl)-alt-(3,3''-di(2-octyldodecyl)-2,2';5',2'';5'',2'''-quaterthiophen-5,5'''-diyl)] (PffBT4T-2OD, **Figure 4d**). The energetic disorder of the high-efficiency



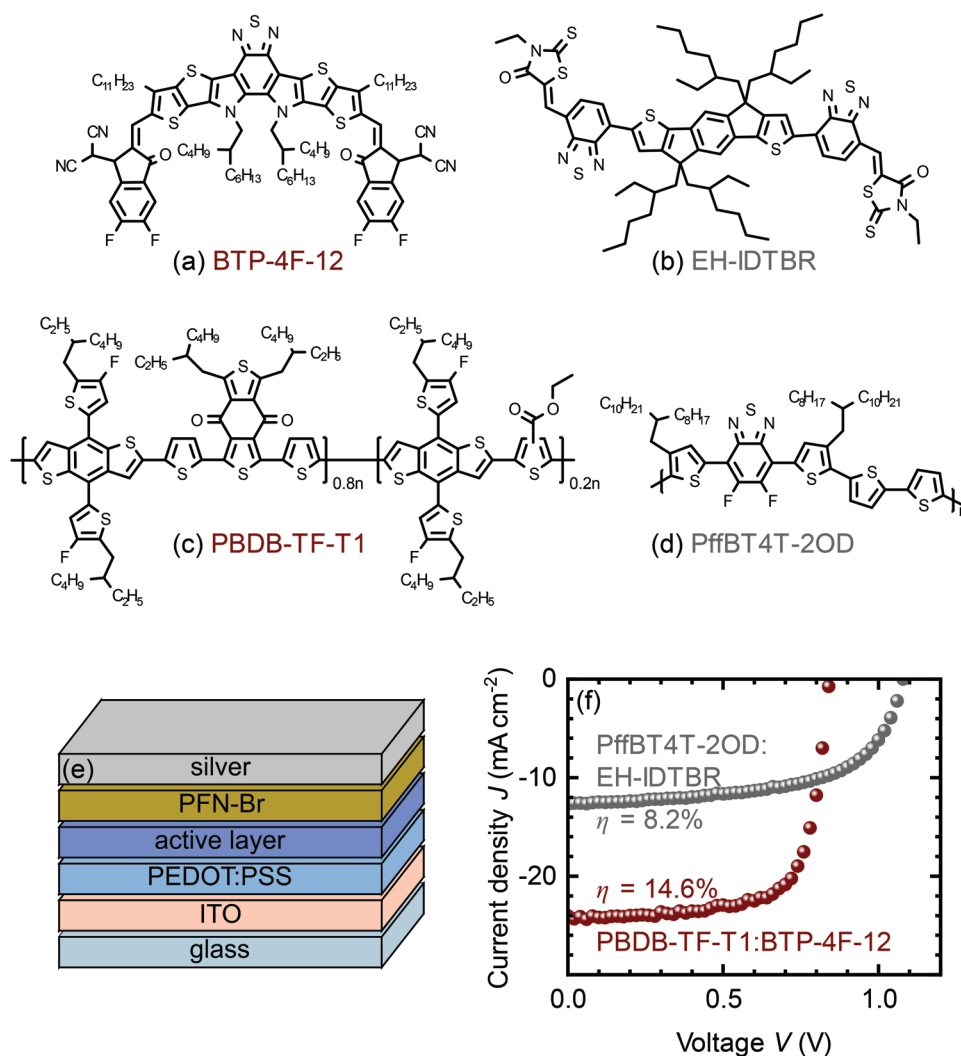


**Figure 4.** a,b) Nonfullerene acceptors and c,d) polymer donors used for solar cell production in the e) device architecture glass/ITO/PEDOT:PSS/active layer/PFN-Br/Ag. f) Current density  $J$  as a function of voltage  $V$  of the two organic solar cells incorporating the bulk heterojunctions PffBT4T-2OD:EH-IDTBR and PBDB-TF-T1:BTP-4F-12 that are characterized in this work. Urbach energies reported in the literature for the same or similar blends imply different severity of energetic disorder between the two material systems.

material system PBDB-TF-T1:BTP-4F-12 to the best of our knowledge has not been investigated so far. Similar materials have been found to exhibit a low Urbach energy.<sup>[38,79,92]</sup> As a contrast, we chose PffBT4T-2OD:EH-IDTBR as an active layer blend for which a relatively high Urbach energy of 76 meV has been reported.<sup>[38]</sup> Both solar cells were fabricated on a glass substrate with an indium tin oxide (ITO) anode, and poly(3,4-ethylenedioxythiophene) polystyrene sulfonate (PEDOT:PSS) as the hole transport layer. On top of the active layer, poly-(9,9-bis(3'-(*N,N*-dimethyl)-*N*-ethylammonium-propyl)-2,7-fluorene)-alt-2,7-(9,9-dioctylfluorene)dibromide (PFN-Br) creates the electron transport layer and a silver cathode is used. While a schematic of the entire stack is shown in Figure 4e, further information on the fabrication process of the organic solar cells can be found in Section S5, Supporting Information. Details on the measurement specifications during characterization are listed in Section S6, Supporting Information. Figure 4f shows the  $JV$  characteristics of the resulting devices.

The cell with PffBT4T-2OD:EH-IDTBR exhibits a higher open-circuit voltage due to its higher band gap but significantly less photocurrent than the device with PBDB-TF-T1:BTP-4F-12. However, it is beyond the scope of this work to analyze the various loss mechanisms that set apart the two solar cell systems. Instead, we want to focus on recombination via shallow defect states.

For this purpose, we characterized the absorption properties of the devices with FTPS and of the active layer films with PDS. **Figure 5** shows the normalized signal of the optical measurements on the material systems a) PffBT4T-2OD:EH-IDTBR and b) PBDB-TF-T1:BTP-4F-12. For every measurement, we fitted the exponential regime (solid lines) to extract the Urbach energy  $E_U$  from the slope  $1/E_U$ . Under FTPS, both solar cells show a very steep increase in absorbance which results in an Urbach energy  $E_{U,FTPS}$  of around 26 meV for PffBT4T-2OD:EH-IDTBR and 23 meV for PBDB-TF-T1:BTP-4F-12. While the FTPS measurements show a dynamic range

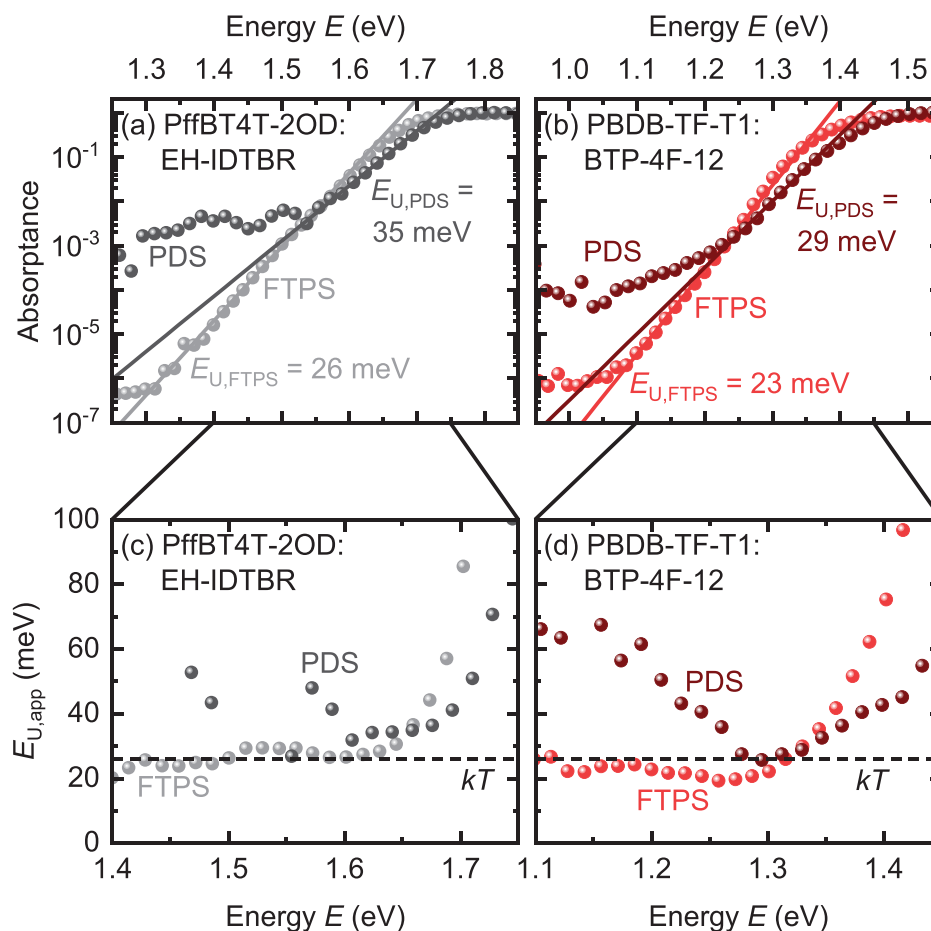


**Figure 5.** Normalized signal of Fourier-transform photocurrent spectroscopy (FTPS) in the lighter colors and photothermal deflection spectroscopy (PDS) in the darker colors as a function of energy  $E$  for organic solar cells based on a,c) PffBT4T-2OD:EH-IDTBR and b,d) PBDB-TF-T1:BTP-4F-12. The solid lines represent fits to the exponential regime of the experimental data with the slope of  $1/E_U$ . c,d) Apparent Urbach energy  $E_{U,app}$ , the inverse logarithmic slope of the absorbance, for both measurement techniques and material systems. Even though scattering becomes more apparent in the  $E_{U,app}$ , both the differential slope and the exponential fit yield Urbach energies close to the thermal energy.

of around six orders of magnitude, PDS has a lower range between two and three orders of magnitude. Therefore, the exponential part of the signal could be affected by the saturation at higher energy resulting in higher Urbach energies  $E_{U,PDS}$  of 35 meV for PffBT4T-2OD:EH-IDTBR, and 29 meV for PBDB-TF-T1:BTP-4F-12. Similarly, we could also observe in our literature research that some of the higher values reported for the Urbach energy from optical measurements could potentially be attributed to the low dynamic range of the measurements.<sup>[30,31,53,58]</sup> Also, the films on glass that were measured for PDS lack absorption from back reflection on the silver cathode that is included in the FTPS measurements causing a further discrepancy between the two methods. On the one hand, the light traverses twice through the absorber layer in FTPS measurements, on the other hand, interference effects can cause differences in the subgap slope.<sup>[107,108]</sup> Still, both optical measurements yield relatively low Urbach energies close to thermal energy. This finding coincides well with the model proposed by Kaiser et al., in which they attribute parts of the subgap absorption features to thermal broadening.<sup>[107]</sup> To better distinguish between the effects of static disorder in the singlet state,

thermal broadening, and deep defects, they plot the apparent Urbach energy  $E_{U,app} = \left( \frac{d \ln(a)}{dE} \right)^{-1}$ , where  $a$  is the absorbance, as a function of energy. Figure 5c,d shows the apparent Urbach energy  $E_{U,app}$  for PDS and FTPS measurements on both material systems. For the measurements on PffBT4T-2OD:EH-IDTBR in Figure 5c, the PDS signal first decreases going from high energies to low energies but does not reach the thermal energy before the limitation in dynamic range causes it to increase again. The FTPS measurements allow further analysis due to the higher dynamic range even though the inverse slope  $E_{U,app}$  is noisy. It exhibits a plateau around thermal energy and higher apparent Urbach energies  $E_{U,app}$  near the optical band edge that can be assigned to the static disorder of the singlet state.<sup>[107]</sup> The apparent Urbach energy  $E_{U,app}$  for PBDB-TF-T1:BTP-4F-12 in Figure 5d behaves similarly. The PDS data features a minimum at thermal energy, whereas the FTPS data further decreases below the value assigned to thermal broadening. As discussed by Kaiser et al., small variations around  $kT$  can be caused by interference effects.<sup>[107]</sup> Kay et al. further observed that the conventional device structure, which is also

employed in our samples, is most susceptible to interference effects.<sup>[108]</sup> Thus, interference could be a possible explanation for apparent Urbach energies  $E_{U,app}$  below thermal energy. Note that the increase in apparent Urbach energy  $E_{U,app}$  in the low energy regime is not an indicator for deep traps in our samples but simply caused by the limit in the dynamic range of the measurements. Therefore, the exponential fits that we applied to the data in Figure 5a,b according to the traditional approach potentially only fit thermal broadening and contain no material-specific information. This observation based on the findings of Kaiser et al. also offers another explanation for why literature values for optically extracted Urbach energies mostly are very low, below 30 meV. A majority of the values above 30 meV that we found in literature either fit features like the charge-transfer state<sup>[85]</sup> or deep defects,<sup>[7,32,54,61,65,66,77,84,85]</sup> or the disorder of the singlet state.<sup>[55,80]</sup> As illustrated in Figure S9, Supporting Information, organic solar cells comprising fullerene acceptors are more frequently reported to have Urbach energies above thermal energy which can be attributed to their typically high energy offsets and more pronounced charge-transfer state absorption.<sup>[107]</sup> Therefore, fitting the subgap absorption with an exponential function is highly sensitive to the fitting range. As an alternative approach, Kay et al. proposed fitting the data with the model of Kaiser et al. to extract the standard deviation of the Gaussian disorder of the singlet state.<sup>[108]</sup> In Figure S10, Supporting Information, we show such a fit to our FTPS data. Contrary to previous observations, it yields a higher disorder with a standard deviation of 41.9 meV for the PBDB-TF-T1:BTP-4F-12 based solar cells than the PffBT4T-2OD:EH-IDTBR-based ones with 35.8 meV. However, the quality of the fit is worse for the first one since the model fails to replicate the apparent Urbach energies  $E_{U,app}$  below  $kT$ . Nonetheless, values extracted for the static disorder in these material systems are relatively low.

For the voltage-dependent method, we performed admittance spectroscopy on the same solar cells that were characterized by FTPS. From the experimental admittance data, we calculated the capacitance  $C - C_{geo}$  as discussed previously as an estimate for the chemical capacitance  $C_{\mu}$ . Figure 6a shows the resulting capacitance as a function of open-circuit voltage  $V_{oc}$  for both

solar cells based on PffBT4T-2OD:EH-IDTBR and PBDB-TF-T1:BTP-4F-12. At low voltages, the capacitance increases before falling at higher voltages. When fitting an exponential function to the increase, one can extract an Urbach energy  $E_{U,CVi} = 55$  meV for PBDB-TF-T1:BTP-4F-12 from the data and  $E_{U,CVi} = 202$  meV for PffBT4T-2OD:EH-IDTBR. The capacitance  $C - C_{geo}$  in the dark in Figure 6b behaves similarly resulting in  $E_{U,CVd} = 49$  meV and  $E_{U,CVd} = 146$  meV for PBDB-TF-T1:BTP-4F-12 and PffBT4T-2OD:EH-IDTBR, respectively. Therefore, the tail slope extracted from voltage-dependent admittance measurements is more than twice as high for PBDB-TF-T1:BTP-4F-12 as the one from optical measurements. This difference appears to be well in line with our observation on Urbach energies reported in the literature. The values extracted from fits of the capacitance of the PffBT4T-2OD:EH-IDTBR solar cell, however, are higher than any typically reported in the literature.

This difference between the methods cannot be explained by including the reorganization energy in the interpretation. For example, one might expect the reorganization energy in optical measurements, where excitonic states or the charge-transfer state are probed, to be different from the reorganization energy of polarons which are considered in electrical measurements. However, while optical techniques measure both the reorganization energy and static disorder,<sup>[20,21,23]</sup> electrical methods only measure the filling of the lowest excited state with electrons and the highest ground state with holes. So, as there is no charge transfer needed between the states, the reorganization energy of polarons is not reflected in the capacitance data. Therefore, this consideration would even lead to higher disorder measured by optical characterization contrary to what we observed in our experiments and in the literature. To understand these inconsistencies between measurement techniques, we further used drift-diffusion simulations to study possible origins leading to higher Urbach energies from voltage-dependent measurements. As the drastic difference in Urbach energy  $E_{U,CV}$  between the two material systems suggests that different effects may occur in the two devices, we will in the following look at the solar cells based on PBDB-TF-T1:BTP-4F-12 and PffBT4T-2OD:EH-IDTBR separately.

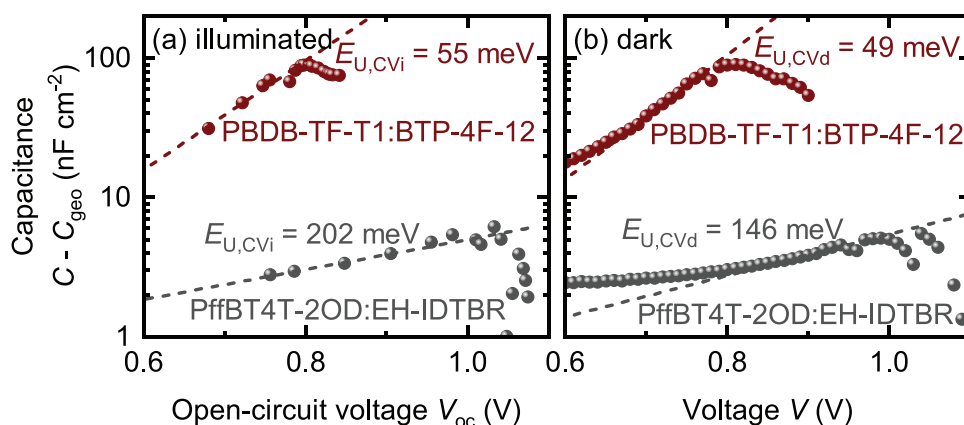


**Figure 6.** Capacitance  $C - C_{geo}$  estimated from admittance spectroscopy measurements a) under illumination at open circuit and b) in the dark on organic solar cells with an active layer consisting of PffBT4T-2OD:EH-IDTBR or PBDB-TF-T1:BTP-4F-12. The dashed lines represent exponential fits to the experimental data with a slope of  $1/(2E_{U,CV})$ . The Urbach energy  $E_{U,CV}$  extracted from the fits for PBDB-TF-T1:BTP-4F-12 is about twice as high as for the optical measurements whereas the values for PffBT4T-2OD:EH-IDTBR are unrealistically high.

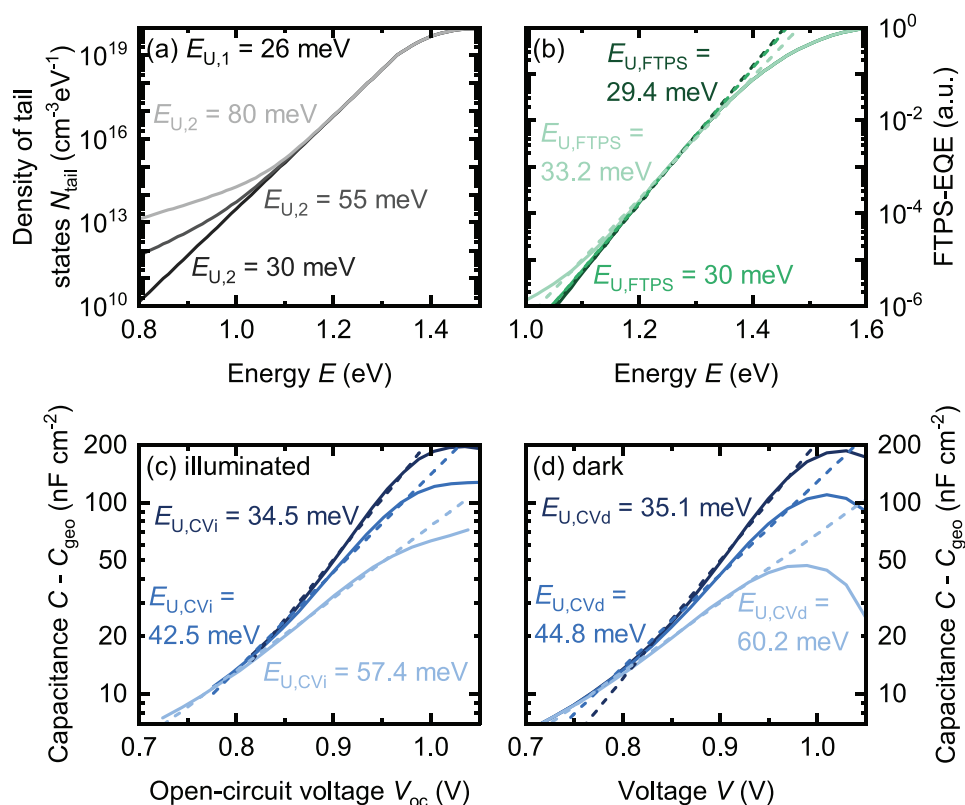


**Figure 7.** a) Total density of states modeled with a combination of a steep Urbach tail with  $E_{U,1} = 26$  meV that dominates near the band edge and a tail with higher Urbach energies  $E_{U,2}$  of 30, 55, or 80 meV that dominates at lower energies  $E$ . b) FTPS-signal calculated from the density of states with two exponential tails. c) Corresponding simulated capacitance  $C - C_{\text{geo}}$  under open-circuit conditions and d) in the dark. The Urbach energies extracted from the dashed fits of the capacitance measurements show more sensitivity to the slope of the deeper tail than for the optical measurements.

## 4. Discussion

We first focus on the effect observed in the PBDB-TF-T1:BTP-4F-12 cells. For this purpose, we modeled a solar cell with a density of tail states consisting of two tails with different slopes and trap density of states. **Figure 7a** shows the resulting density of tail states for a steep Urbach tail with  $E_{U,1} = 26$  meV that dominates close to the band edge and a more shallow tail with varying Urbach energy  $E_{U,2}$  of 30, 55, and 80 meV that dominates further in the band. The FTPS signal that can be calculated from this density of states is displayed in **Figure 7b**. In the range that can be resolved by the measurement, there is only little influence by the deep tail. Therefore, the Urbach energy  $E_{U,\text{FTPS}}$  that could be extracted from these optical measurements only ranges from 29 to 33 meV. In contrast, the admittance measurements in **Figure 7c,d** are more sensitive to the variation of the deep Urbach tail and result in significantly different fits. Therefore, at the voltages applied to the solar cell, these deep tails are still filled with increasing voltage. So, with the filling according to the quasi-Fermi levels, an energy range of the density of states is probed that can be below the resolution of FTPS measurements. Thereby, the voltage-dependent measurements can in fact show features of deeper traps in the device. Hence, the difference in Urbach energy between optical and voltage-dependent measurements as observed for PBDB-TF-T1:BTP-4F-12 can originate in probing

a density of trap states at different energy ranges that are not monoexponential.

Yet, for this effect to evoke Urbach energies  $E_{U,\text{CV}}$  as high as observed for PffBT4T-2OD:EH-IDTBR, the slope of the density of deep defect states would need to be extremely low. Therefore, we need to further study the chemical capacitance of this material system and explore the possibility that it does not actually reflect the density of states. As seen in **Figure 4f**, the solar cell based on PffBT4T-2OD:EH-IDTBR only shows a power-conversion efficiency of around 8%. The material system is known to have poor charge-carrier mobilities<sup>[109]</sup> and due to different energy levels compared to PBDB-TF-T1:BTP-4F-12, the injection barriers might differ. In addition, even though the density of states seems to be steeply close to the band edge, recombination via these tail states can still be high due to high capture rates. Even the increased active layer thickness, which is around 150 nm for this solar cell, can lead to transport issues and space-charge effects due to less uniform charge-carrier generation. The effect of the injection barriers, the capture rates, and the active layer thickness on the capacitance-voltage curves predicted by simulations is shown in **Figure S8**, Supporting Information. In the following, we will focus only on charge-carrier mobility as an example.

**Figure 8** shows the simulation results for an Urbach energy  $E_{U,\text{CV}}$  of 30 meV but different charge-carrier mobilities  $\mu$  to illustrate how limited transport can cause the experimental



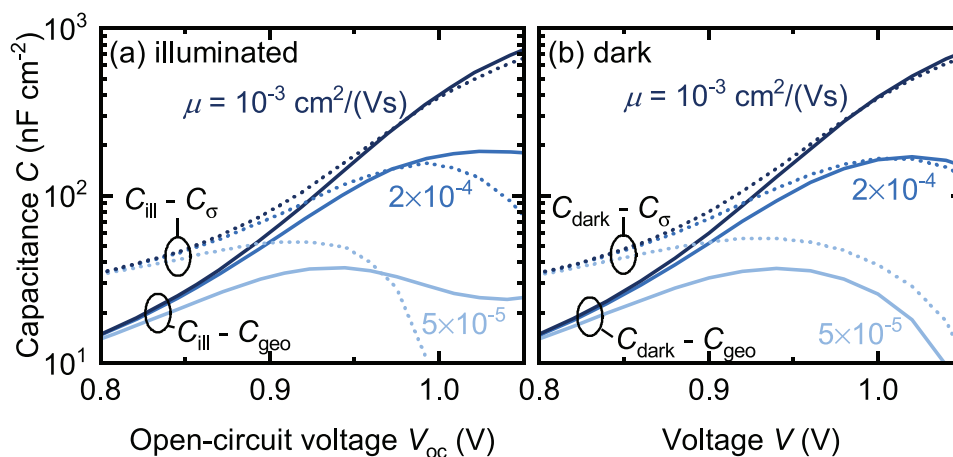


**Figure 8.** Simulated capacitance a) at open circuit under varying illumination intensity and b) in the dark for different applied voltages  $V$  and multiple charge-carrier mobilities  $\mu$ . The solid lines represent the difference between the total capacitance and the geometric capacitance  $C_{\text{geo}}$ , which is an estimate of the chemical capacitance that can be determined experimentally. The curves flatten for lower mobilities. The dotted lines are the difference between the total capacitance and the electrode capacitance  $C_{\sigma}$ , which is the best approximation for  $C_{\mu}$  but can only be extracted from simulations. The issue of flat CV curves does not originate in the assumption  $C_{\sigma} \approx C_{\text{geo}}$ , since both approaches show a similar behavior at high voltages with decreasing charge-carrier mobility.

trends observed in Figure 6. Once more, it shows the chemical capacitance at a) open circuit and b) in the dark estimated by the difference between the total capacitance and the geometric capacitance  $C_{\text{geo}}$  with the solid lines. It appears that under both working conditions, the curves are flattening with decreasing mobilities. Therefore, at low charge-carrier mobilities, the Urbach energy  $E_{\text{U,CV}}$  calculated from the slope of the graphs would be an overestimation. There are several assumptions underlying this estimation. One of them is the calculation of the chemical capacitance as the difference  $C - C_{\text{geo}}$  of the total capacitance and the constant geometric capacitance  $C_{\text{geo}}$  as discussed in Section S4, Supporting Information. It assumes that the charge on the electrodes that contributes to the geometric capacitance  $C_{\text{geo}}$  is constant over the entire voltage range. In reality, the electrode capacitance can be voltage-dependent. Therefore, for the true chemical capacitance, one needs to subtract the voltage-dependent electrode capacitance  $C_{\sigma}$ . Even though  $C_{\sigma}$  is not experimentally accessible, we can extract it from the drift-diffusion simulations. Consequently, Figure 8 shows  $C - C_{\sigma}$  with the dashed lines for comparison. It reveals the same trend with mobility as the experimentally accessible  $C - C_{\text{geo}}$ . So, the flattening of the CV curves does not originate in capacitive but rather resistive effects.

**Figure 9** illustrates how a series resistance  $R_s$  inside the active layer causes the flattening of the capacitance-voltage curves. In Figure 9a, the dark current density is plotted for an organic solar cell with high mobilities and one with low mobilities. Even though external resistances are neglected in the simulations, the current density increases less rapidly at high voltages, typical for a series resistance. This behavior indicates that the limited mobility causes an internal series resistance  $R_s$  that increases with decreasing charge-carrier mobility. Therefore, the simple RC circuit that was used so far for the determination of the total capacitance as the imaginary part of the admittance  $Y$  must be extended by a series resistance. The resulting equivalent circuit is shown in Figure 9b. While the series resistance

$R_s$  can be roughly estimated by fitting the dark JV curves with the diode equation, the two other circuit elements, the chemical capacitance  $C_{\mu}$  and the recombination resistance  $R_{\text{rec}}$ , can also be obtained from steady-state quantities given by the simulations. Estimation of all circuit elements allows us to calculate the effective capacitance  $C_{\text{eff,cir}}$  that we would get if the equivalent circuit in Figure 9b was true, but we still assumed  $C_{\text{eff,cir}} = \text{Im}(Y)/\omega$ , where  $\omega$  is the angular frequency. For further details on the calculation of  $C_{\text{eff,cir}}$ , see Section S7, Supporting Information. Figure 9c shows this effective capacitance  $C_{\text{eff,cir}}$  for the high and low mobility  $\mu$  alongside the capacitance  $C - C_{\sigma}$  that was discussed in Figure 8b. The latter is given by the imaginary part of the admittance simulated under alternating current. In fact, the effective capacitance  $C_{\text{eff,cir}}$  based on the circuit in Figure 9b replicates the decreasing capacitance  $C - C_{\sigma}$  very well. The chemical capacitance  $C_{\mu,\text{ana}}$  calculated analytically from steady-state quantities shows that the chemical capacitance itself is not dropping. Only the inclusion of the series resistance  $R_s$  allows for a drop in effective capacitance. Therefore, all quantities that hinder transport and thereby cause an internal series resistance  $R_s$  will lead to an early decrease in the effective capacitance and therefore an overestimation of the Urbach energy  $E_{\text{U,CV}}$ . Herein, we have demonstrated how the shape of the capacitance-voltage curves can be dominated by resistive effects. This observation is relevant independent of the actual underlying shape of the subgap density of states and the model applied to it. As illustrated in Figure S11, Supporting Information, for a Gaussian density of states, we observe the same trend with mobility as discussed for exponential tail states. In contrast, transport issues are not relevant for the PDS measurement and are much less significant in FTPS measurements due to the stronger internal electric field under the operation at short circuit. Thus, the high susceptibility of admittance measurements to bad electronic properties can lead to discrepancies in the reported Urbach energy compared to the less sensitive optical measurements.

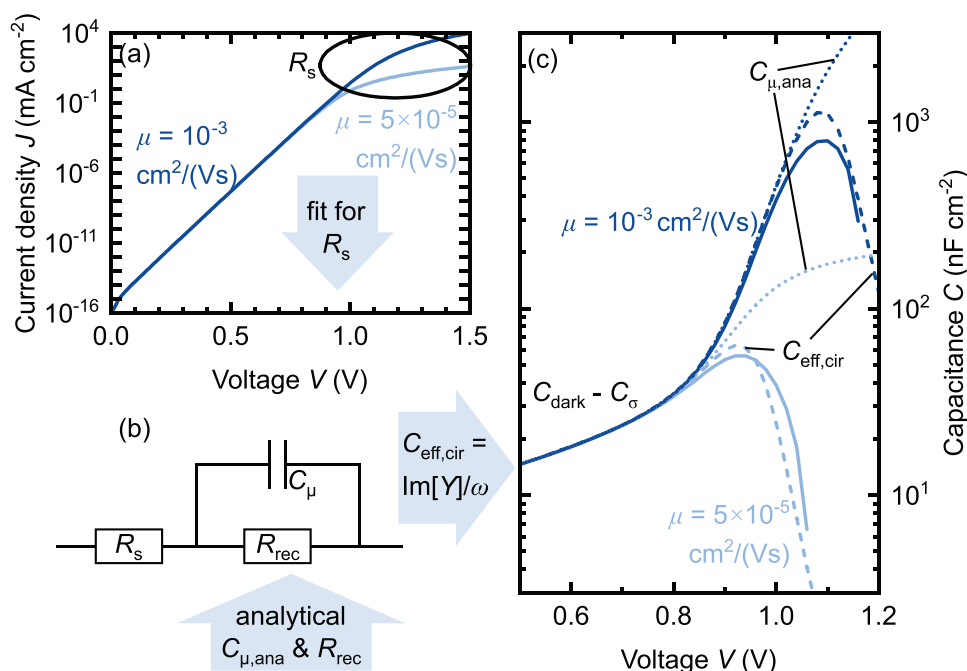


**Figure 9.** a) Dark JV-characteristic of organic solar cells with high and low charge-carrier mobilities  $\mu$  and no external resistance. The high-voltage regime indicates an internal series resistance  $R_s$ . b) Equivalent circuit model extended by the internal series resistance  $R_s$  which can be estimated from fitting the dark JV-curve. The chemical capacitance  $C_{\mu,ana}$  and the recombination resistance  $R_{rec}$  can be calculated from steady-state quantities using analytical expressions. c) Dark capacitance-voltage characteristics for high and low mobilities  $\mu$ . The effective capacitance  $C_{eff,cir}$  with the dashed lines calculated from the equivalent circuit fits well with the chemical capacitance  $C - C_\sigma$  given by the drift-diffusion simulations. The constant increase in the dotted analytical chemical capacitance  $C_{\mu,ana}$  proves that the internal series resistance  $R_s$  is needed to explain the drop in the simulated capacitance.

## 5. Conclusions

The characterization of energetic disorder plays an important role in the search for material systems that enable high-efficiency organic solar cells. Optical methods are often used for this purpose where electrons are excited from or into defect states by incident photons. For instance, PDS,<sup>[29–31]</sup> FTPS,<sup>[32,33]</sup> or highly sensitive external quantum efficiency (EQE) measurements<sup>[34,35]</sup> are frequently applied in the literature. But apart from these absorption-based methods, the density of defect states can also be probed by varying the quasi-Fermi level splitting with an applied voltage in, for example, charge extraction<sup>[36–38]</sup> or admittance measurements.<sup>[39]</sup> We found that both in the literature and our experiments, these electrical, voltage-dependent measurements yield overall higher Urbach energies than the techniques based on optical excitation. We conducted optical FTPS and PDS measurements and electrical admittance spectroscopy under illumination and in the dark on two NFA-based material systems. In all cases, the Urbach energy extracted by the voltage-dependent methods was at least twice as high as its optical counterparts.

In our analysis, we show that care must be taken when analyzing experimental data as different effects can be mistakenly interpreted as features of the energetic disorder. Even for purely optical data, we have observed that a low dynamic range in PDS measurements can lead to a lower slope at the band edge than in FTPS on the same material. Voltage-dependent admittance measurements have proven to be even more delicate as the analysis in terms of energetic disorder is based on a high number

of assumptions. Our experimental and simulation results on the extreme case of a solar cell based on PffBT4T-2OD:EH-IDTBR have demonstrated how bad transport properties can lead to an internal series resistance overlaying the exponential regime of the capacitance-voltage measurements. Thereby, the discrepancy in the Urbach energy between optical and voltage-dependent measurements can originate in an overestimation in voltage-dependent measurements due to bad electronic properties.

Knowing the limitations of the characterization techniques, we have also highlighted the potential that both optical and electrical methods correctly reflect the subband-gap density of states even though they yield different values for the Urbach energy. Moving away from a strictly monoexponential band tail, we have shown that the quasi-Fermi level splitting that is typical for voltage-dependent measurements probes energy ranges of the density of states where the signal of the optical measurements is below its resolution. Therefore, different approaches may detect different features of a density of defect states.

So, we recommend the combination of different characterization techniques not only to be able to minimize the chance of unknowingly running into the limitations of a method but also to maximize the information gained on the energetic disorder in organic solar cells.

## Supporting Information

Supporting Information is available from the Wiley Online Library or from the author.

## Acknowledgements

The authors acknowledge funding from the Helmholtz Association. S.R. acknowledges the German Research Foundation (DFG) for support through a Walter-Benjamin fellowship (Project No. 462572437).

Open access funding enabled and organized by Projekt DEAL.

## Conflict of Interest

The authors declare no conflict of interest.

## Data Availability Statement

The data that support the findings of this study are available from the corresponding author upon reasonable request.

## Keywords

impedance spectroscopy, organic photovoltaics, shallow defects, tail states, Urbach energy

Received: February 1, 2023  
Published online: March 2, 2023

- [1] T. Matsui, A. Bidiville, K. Maejima, H. Sai, T. Koida, T. Suezaki, M. Matsumoto, K. Saito, I. Yoshida, M. Kondo, *Appl. Phys. Lett.* **2015**, *106*, 053901.
- [2] O. Almora, D. Baran, G. C. Bazan, C. Berger, C. I. Cabrera, K. R. Catchpole, S. Erten-Ela, F. Guo, J. Hauch, A. W. Y. Ho-Baillie, T. J. Jacobsson, R. A. J. Janssen, T. Kirchartz, N. Kopidakis, Y. Li, M. A. Loi, R. R. Lunt, X. Mathew, M. D. McGehee, J. Min, D. B. Mitzi, M. K. Nazeeruddin, J. Nelson, A. F. Nogueira, U. W. Paetzold, N. G. Park, B. P. Rand, U. Rau, H. J. Snaith, E. Unger, et al., *Adv. Energy Mater.* **2021**, *11*, 2102526.
- [3] S. Benagli, D. Borrello, E. Vallat-Sauvain, J. Meier, U. Kroll, J. Hötzel, J. Bailat, J. Steinhauser, M. Marmelo, G. Monteduro, in *24th European Photovoltaic Solar Energy Conf.*, Hamburg, Germany, **2009**, 21, <https://doi.org/10.4229/24thEUPVSEC2009-3BO.9.3>.
- [4] P. K. Nayak, G. Garcia-Belmonte, A. Kahn, J. Bisquert, D. Cahen, *Energy Environ. Sci.* **2012**, *5*, 6022.
- [5] T. Tiedje, *Appl. Phys. Lett.* **1982**, *40*, 627.
- [6] T. Tiedje, J. M. Cebulka, D. L. Morel, B. Abeles, *Phys. Rev. Lett.* **1981**, *46*, 1425.
- [7] S. A. Hawks, G. Li, Y. Yang, R. A. Street, *J. Appl. Phys.* **2014**, *116*, 074503.
- [8] G. Garcia-Belmonte, J. Bisquert, *Appl. Phys. Lett.* **2010**, *96*, 113301.
- [9] M. Tachiya, K. Seki, *Phys. Rev. B* **2010**, *82*, 085201.
- [10] A. Armin, W. Li, O. J. Sandberg, Z. Xiao, L. Ding, J. Nelson, D. Neher, K. Vandewal, S. Shoaee, T. Wang, H. Ade, T. Heumüller, C. Brabec, P. Meredith, *Adv. Energy Mater.* **2021**, *11*, 2003570.
- [11] Y. Cui, Y. Xu, H. Yao, P. Bi, L. Hong, J. Zhang, Y. Zu, T. Zhang, J. Qin, J. Ren, Z. Chen, C. He, X. Hao, Z. Wei, J. Hou, *Adv. Mater.* **2021**, *33*, 2102420.
- [12] W. Gao, F. Qi, Z. Peng, F. R. Lin, K. Jiang, C. Zhong, W. Kaminsky, Z. Guan, C. S. Lee, T. J. Marks, H. Ade, A. K. Jen, *Adv. Mater.* **2022**, *34*, 2202089.
- [13] C. He, Y. Pan, Y. Ouyang, Q. Shen, Y. Gao, K. Yan, J. Fang, Y. Chen, C.-Q. Ma, J. Min, C. Zhang, L. Zuo, H. Chen, *Energy Environ. Sci.* **2022**, *15*, 2537.
- [14] Y. Wei, Z. Chen, G. Lu, N. Yu, C. Li, J. Gao, X. Gu, X. Hao, G. Lu, Z. Tang, J. Zhang, Z. Wei, X. Zhang, H. Huang, *Adv. Mater.* **2022**, *34*, 2204718.
- [15] L. Zhu, M. Zhang, J. Xu, C. Li, J. Yan, G. Zhou, W. Zhong, T. Hao, J. Song, X. Xue, Z. Zhou, R. Zeng, H. Zhu, C. C. Chen, R. C. I. MacKenzie, Y. Zou, J. Nelson, Y. Zhang, Y. Sun, F. Liu, *Nat. Mater.* **2022**, *21*, 656.
- [16] Z. Zheng, J. Wang, P. Bi, J. Ren, Y. Wang, Y. Yang, X. Liu, S. Zhang, J. Hou, *Joule* **2021**, *6*, 171.
- [17] J. M. Frost, J. Kirkpatrick, T. Kirchartz, J. Nelson, *Faraday Discuss.* **2014**, *174*, 255.
- [18] M. Fox, in *Optical Properties of Solids*, Vol. 3, Oxford University Press, Oxford **2002**, Ch. 8.
- [19] K. Vandewal, K. Tvingstedt, A. Gadisa, O. Inganäs, J. V. Manca, *Phys. Rev. B* **2010**, *81*, 125204.
- [20] J. Yan, E. Rezasoltani, M. Azzouzi, F. Eisner, J. Nelson, *Nat. Commun.* **2021**, *12*, 3642.
- [21] K. Tvingstedt, J. Benduhn, K. Vandewal, *Mater. Horiz.* **2020**, *7*, 1888.
- [22] T. M. Burke, S. Sweetnam, K. Vandewal, M. D. McGehee, *Adv. Energy Mater.* **2015**, *5*, 1500123.
- [23] F.-J. Kahle, A. Rudnick, H. Bässler, A. Köhler, *Mater. Horiz.* **2018**, *5*, 837.
- [24] G. D. Cody, T. Tiedje, B. Abeles, B. Brooks, Y. Goldstein, *Phys. Rev. Lett.* **1981**, *47*, 1480.
- [25] C. Göhler, M. Saladina, Y. Wang, D. Spoltore, J. Benduhn, K. Leo, C. Deibel, *Phys. Rev. Appl.* **2021**, *15*, 064009.
- [26] T. Kirchartz, B. E. Pieters, J. Kirkpatrick, U. Rau, J. Nelson, *Phys. Rev. B* **2011**, *83*, 115209.
- [27] J. Benduhn, K. Tvingstedt, F. Piersimoni, S. Ullbrich, Y. Fan, M. Tropicano, K. A. McGarry, O. Zeika, M. K. Riede, C. J. Douglas, S. Barlow, S. R. Marder, D. Neher, D. Spoltore, K. Vandewal, *Nat. Energy* **2017**, *2*, 17053.
- [28] M. Azzouzi, J. Yan, T. Kirchartz, K. Liu, J. Wang, H. Wu, J. Nelson, *Phys. Rev. X* **2018**, *8*, 031055.
- [29] C. Zhang, J. Yuan, J. K. W. Ho, J. Song, H. Zhong, Y. Xiao, W. Liu, X. Lu, Y. Zou, S. K. So, *Adv. Funct. Mater.* **2021**, *31*, 2101627.
- [30] H. Yin, S. Chen, P. Bi, X. Xu, S. H. Cheung, X. Hao, Q. Peng, X. Zhu, S. K. So, *Org. Electron.* **2019**, *65*, 156.
- [31] C. Xu, M. Wright, D. Ping, H. Yi, X. Zhang, M. A. Mahmud, K. Sun, M. B. Upama, F. Haque, A. Uddin, *Org. Electron.* **2018**, *62*, 261.
- [32] L. Zhang, W. Deng, B. Wu, L. Ye, X. Sun, Z. Wang, K. Gao, H. Wu, C. Duan, F. Huang, Y. Cao, *ACS Appl. Mater. Interfaces* **2020**, *12*, 753.
- [33] C. He, Y. Li, Y. Liu, Y. Li, G. Zhou, S. Li, H. Zhu, X. Lu, F. Zhang, C.-Z. Li, H. Chen, *J. Mater. Chem. A* **2020**, *8*, 18154.
- [34] A. Karki, J. Vollbrecht, A. J. Gillett, P. Selter, J. Lee, Z. Peng, N. Schopp, A. L. Dixon, M. Schrock, V. Nádaždy, F. Schauer, H. Ade, B. F. Chmelka, G. C. Bazan, R. H. Friend, T. Q. Nguyen, *Adv. Energy Mater.* **2020**, *10*, 2001203.
- [35] P. K. Nayak, S. Mahesh, H. J. Snaith, D. Cahen, *Nat. Rev. Mater.* **2019**, *4*, 269.
- [36] J. Wu, J. Luke, H. K. H. Lee, P. S. Tuladhar, H. Cha, S.-Y. Jang, W. C. Tsoi, M. Heeney, H. Kang, K. Lee, T. Kirchartz, J.-S. Kim, J. R. Durrant, *Nat. Commun.* **2019**, *10*, 5159.
- [37] C. Deibel, D. Rauh, A. Foertig, *Appl. Phys. Lett.* **2013**, *103*, 043307.
- [38] J. Wu, J. Lee, Y.-C. Chin, H. Yao, H. Cha, J. Luke, J. Hou, J.-S. Kim, J. R. Durrant, *Energy Environ. Sci.* **2020**, *13*, 2422.
- [39] S. D. Collins, C. M. Proctor, N. A. Ran, T.-Q. Nguyen, *Adv. Energy Mater.* **2016**, *6*, 1501721.
- [40] H. Wang, Z. Zhang, J. Yu, P. C. Lin, C. C. Chueh, X. Liu, S. Guang, S. Qu, W. Tang, *ACS Appl. Mater. Interfaces* **2020**, *12*, 21633.
- [41] N. A. Ran, J. A. Love, M. C. Heiber, X. Jiao, M. P. Hughes, A. Karki, M. Wang, V. V. Brus, H. Wang, D. Neher, H. Ade, G. C. Bazan, T.-Q. Nguyen, *Adv. Energy Mater.* **2018**, *8*, 1701073.

- [42] R. A. Street, Y. Yang, B. C. Thompson, I. McCulloch, *J. Phys. Chem. C* **2016**, 120, 22169.
- [43] M. Soldera, K. Taretto, T. Kirchartz, *Phys. Status Solidi A* **2012**, 209, 207.
- [44] J. Yan, Q. Liang, K. Liu, J. Miao, H. Chen, S. Liu, Z. He, H. Wu, J. Wang, Y. Cao, *ACS Energy Lett.* **2016**, 2, 14.
- [45] A. Maurano, C. G. Shuttle, R. Hamilton, A. M. Ballantyne, J. Nelson, W. Zhang, M. Heeney, J. R. Durrant, *J. Phys. Chem. C* **2011**, 115, 5947.
- [46] T. Ripolles-Sanchis, S. R. Raga, A. Guerrero, M. Welker, M. Turbiez, J. Bisquert, G. Garcia-Belmonte, *J. Phys. Chem. C* **2013**, 117, 8719.
- [47] L. Duan, H. Yi, Y. Zhang, F. Haque, C. Xu, A. Uddin, *Sustainable Energy Fuels* **2019**, 3, 723.
- [48] T. F. Hinrichsen, C. C. S. Chan, C. Ma, D. Palecek, A. Gillett, S. Chen, X. Zou, G. Zhang, H. L. Yip, K. S. Wong, R. H. Friend, H. Yan, A. Rao, P. C. Y. Chow, *Nat. Commun.* **2020**, 11, 5617.
- [49] S. Liu, J. Yuan, W. Deng, M. Luo, Y. Xie, Q. Liang, Y. Zou, Z. He, H. Wu, Y. Cao, *Nat. Photonics* **2020**, 14, 300.
- [50] L. Duan, Y. Zhang, H. Yi, C. Xu, F. Haque, A. Uddin, in 2019 IEEE 46th Photovoltaic Specialists Conf. (PVSC), IEEE, Piscataway, NJ **2019**, 0461.
- [51] W. Gong, M. A. Faist, N. J. Ekins-Daukes, Z. Xu, D. D. C. Bradley, J. Nelson, T. Kirchartz, *Phys. Rev. B* **2012**, 86, 024201.
- [52] N. A. Ran, J. A. Love, C. J. Takacs, A. Sadhanala, J. K. Beavers, S. D. Collins, Y. Huang, M. Wang, R. H. Friend, G. C. Bazan, T. Q. Nguyen, *Adv. Mater.* **2016**, 28, 1482.
- [53] H. Yin, S. H. Cheung, J. H. L. Ngai, C. H. Y. Ho, K. L. Chiu, X. Hao, H. W. Li, Y. Cheng, S. W. Tsang, S. K. So, *Adv. Electron. Mater.* **2017**, 3, 1700007.
- [54] N. Felekidis, A. Melianas, M. Kemerink, *J. Phys. Chem. Lett.* **2020**, 11, 3563.
- [55] N. Chandrasekaran, E. Gann, N. Jain, A. Kumar, S. Gopinathan, A. Sadhanala, R. H. Friend, A. Kumar, C. R. McNeill, D. Kabra, *ACS Appl. Energy Mater.* **2016**, 8, 20243.
- [56] W. Deng, K. Gao, J. Yan, Q. Liang, Y. Xie, Z. He, H. Wu, X. Peng, Y. Cao, *ACS Appl. Mater. Interfaces* **2018**, 10, 8141.
- [57] N. Jain, U. Bothra, D. Moghe, A. Sadhanala, R. H. Friend, C. R. McNeill, D. Kabra, *ACS Appl. Mater. Interfaces* **2018**, 10, 44576.
- [58] M. B. Upama, M. Wright, B. Puthen-Veetil, N. K. Elumalai, M. A. Mahmud, D. Wang, K. H. Chan, C. Xu, F. Haque, A. Uddin, *RSC Adv.* **2016**, 6, 103899.
- [59] H. Yin, S. Chen, S. H. Cheung, H. W. Li, Y. Xie, S. W. Tsang, X. Zhu, S. K. So, *J. Mater. Chem. C* **2018**, 6, 9111.
- [60] L. Duan, Y. Zhang, H. Yi, F. Haque, C. Xu, S. Wang, A. Uddin, *Mater. Sci. Semicond. Process.* **2020**, 105, 104750.
- [61] R. A. Street, K. W. Song, J. E. Northrup, S. Cowan, *Phys. Rev. B* **2011**, 83, 165207.
- [62] S. M. Menke, A. Sadhanala, M. Nikolka, N. A. Ran, M. K. Ravva, S. Abdel-Azeim, H. L. Stern, M. Wang, H. Sirringhaus, T. Q. Nguyen, J. L. Bredas, G. C. Bazan, R. H. Friend, *ACS Nano* **2016**, 10, 10736.
- [63] R. C. I. MacKenzie, C. G. Shuttle, G. F. Dibb, N. Treat, E. von Hauff, M. J. Robb, C. J. Hawker, M. L. Chabiny, J. Nelson, *J. Phys. Chem. C* **2013**, 117, 12407.
- [64] N. Jain, N. Chandrasekaran, A. Sadhanala, R. H. Friend, C. R. McNeill, D. Kabra, *J. Mater. Chem. A* **2017**, 5, 24749.
- [65] R. A. Street, J. E. Northrup, B. S. Krusor, *Phys. Rev. B* **2012**, 85, 205211.
- [66] R. A. Street, A. Krakaris, S. R. Cowan, *Adv. Funct. Mater.* **2012**, 22, 4608.
- [67] R. A. Street, *Phys. Rev. B* **2011**, 84, 075208.
- [68] Z. M. Bailey, E. T. Hoke, R. Noriega, J. Dacuna, G. F. Burkhard, J. A. Bartelt, A. Salleo, M. F. Toney, M. D. McGehee, *Adv. Energy Mater.* **2011**, 1, 954.
- [69] C. G. Shuttle, A. Maurano, R. Hamilton, B. O'Regan, J. C. de Mello, J. R. Durrant, *Appl. Phys. Lett.* **2008**, 93, 183501.
- [70] A. Maurano, R. Hamilton, C. G. Shuttle, A. M. Ballantyne, J. Nelson, B. O'Regan, W. Zhang, I. McCulloch, H. Azimi, M. Morana, C. J. Brabec, J. R. Durrant, *Adv. Mater.* **2010**, 22, 4987.
- [71] D. Kiermasch, A. Baumann, M. Fischer, V. Dyakonov, K. Tvingstedt, *Energy Environ. Sci.* **2018**, 11, 629.
- [72] P. Yu, A. Migan-Dubois, J. Alvarez, A. Darga, V. Vissac, D. Mencaraglia, Y. Zhou, M. Krueger, *J. Non-Cryst. Solids* **2012**, 358, 2537.
- [73] A. Karki, J. Vollbrecht, A. L. Dixon, N. Schopp, M. Schrock, G. N. M. Reddy, T. Q. Nguyen, *Adv. Mater.* **2019**, 31, 1903868.
- [74] Y. Cui, H. Yao, J. Zhang, K. Xian, T. Zhang, L. Hong, Y. Wang, Y. Xu, K. Ma, C. An, C. He, Z. Wei, F. Gao, J. Hou, *Adv. Mater.* **2020**, 32, 1908205.
- [75] Y. Zhang, G. Cai, Y. Li, Z. Zhang, T. Li, X. Zuo, X. Lu, Y. Lin, *Adv. Mater.* **2021**, 33, 2008134.
- [76] F. Hamada, A. Saeki, *ChemSusChem* **2021**, 14, 3528.
- [77] L. Ma, S. Zhang, H. Yao, Y. Xu, J. Wang, Y. Zu, J. Hou, *ACS Appl. Mater. Interfaces* **2020**, 12, 18777.
- [78] Y. Firdaus, Q. He, Y. Lin, F. A. A. Nugroho, V. M. Le Corre, E. Yengel, A. H. Balawi, A. Seitkhan, F. Laquai, C. Langhammer, F. Liu, M. Heeney, T. D. Anthopoulos, *J. Mater. Chem. A* **2020**, 8, 1164.
- [79] T. Yang, R. Ma, H. Cheng, Y. Xiao, Z. Luo, Y. Chen, S. Luo, T. Liu, X. Lu, H. Yan, *J. Mater. Chem. A* **2020**, 8, 17706.
- [80] X. Chen, B. Kan, Y. Kan, M. Zhang, S. B. Jo, K. Gao, F. Lin, F. Liu, X. Peng, Y. Cao, A. K. Y. Jen, *Adv. Funct. Mater.* **2020**, 30, 1909535.
- [81] L. Duan, M. Guli, Y. Zhang, H. Yi, F. Haque, A. Uddin, *Energy Technol.* **2020**, 8, 1901401.
- [82] G. K. Poduval, L. Duan, M. A. Hossain, B. Sang, Y. Zhang, Y. Zou, A. Uddin, B. Hoex, *Sol. RRL* **2020**, 4, 2000241.
- [83] N. Schopp, V. V. Brus, J. Lee, A. Dixon, A. Karki, T. Liu, Z. Peng, K. R. Graham, H. Ade, G. C. Bazan, T. Q. Nguyen, *Adv. Funct. Mater.* **2021**, 31, 2009363.
- [84] Y. N. Chen, M. Li, Y. Wang, J. Wang, M. Zhang, Y. Zhou, J. Yang, Y. Liu, F. Liu, Z. Tang, Q. Bao, Z. Bo, *Angew. Chem., Int. Ed. Engl.* **2020**, 59, 22714.
- [85] K. Zhou, Y. Liu, A. Alotaibi, J. Yuan, C. Jiang, J. Xin, X. Liu, B. A. Collins, F. Zhang, W. Ma, *ACS Energy Lett.* **2020**, 5, 589.
- [86] L. Duan, Y. Zhang, M. He, R. Deng, H. Yi, Q. Wei, Y. Zou, A. Uddin, *ACS Appl. Mater. Interfaces* **2020**, 12, 27433.
- [87] M. B. Upama, M. Wright, M. A. Mahmud, N. K. Elumalai, A. M. Soufiani, D. Wang, C. Xu, A. Uddin, *Nanoscale* **2017**, 9, 18788.
- [88] A. Yin, D. Zhang, S. H. Cheung, S. K. So, Z. Fu, L. Ying, F. Huang, H. Zhou, Y. Zhang, *J. Mater. Chem. C* **2018**, 6, 7855.
- [89] C. Zhang, J. Yuan, K. L. Chiu, H. Yin, W. Liu, G. Zheng, J. K. W. Ho, S. Huang, G. Yu, F. Gao, Y. Zou, S. K. So, *J. Mater. Chem. A* **2020**, 8, 8566.
- [90] Z. Zhang, Y. Li, G. Cai, Y. Zhang, X. Lu, Y. Lin, *J. Am. Chem. Soc.* **2020**, 142, 18741.
- [91] D. Baran, N. Gasparini, A. Wadsworth, C. H. Tan, N. Wehbe, X. Song, Z. Hamid, W. Zhang, M. Neophytou, T. Kirchartz, C. J. Brabec, J. R. Durrant, I. McCulloch, *Nat. Commun.* **2018**, 9, 2059.
- [92] T. Wang, M. S. Niu, Z. C. Wen, Z. N. Jiang, C. C. Qin, X. Y. Wang, H. Y. Liu, X. Y. Li, H. Yin, J. Q. Liu, X. T. Hao, *ACS Appl. Mater. Interfaces* **2021**, 13, 11134.
- [93] F. Urbach, *Phys. Rev.* **1953**, 92, 1324.
- [94] J. Bisquert, I. Mora-Sero, F. Fabregat-Santiago, *ChemElectroChem* **2014**, 1, 289.
- [95] S. Ravishankar, Z. Liu, U. Rau, T. Kirchartz, *PRX Energy* **2022**, 1, 013003.
- [96] I. Zonno, H. Zayani, M. Grzeslo, B. Krogmeier, T. Kirchartz, *Phys. Rev. Appl.* **2019**, 11, 054024.

- [97] G. Garcia-Belmonte, P. P. Boix, J. Bisquert, M. Sessolo, H. J. Bolink, *Sol. Energy Mater. Sol. Cells* **2010**, *94*, 366.
- [98] V. V. Brus, C. M. Proctor, N. A. Ran, T.-Q. Nguyen, *Adv. Energy Mater.* **2016**, *6*, 1502250.
- [99] M. C. Heiber, T. Okubo, S.-J. Ko, B. R. Luginbuhl, N. A. Ran, M. Wang, H. Wang, M. A. Uddin, H. Y. Woo, G. C. Bazan, T.-Q. Nguyen, *Energy Environ. Sci.* **2018**, *11*, 3019.
- [100] C. M. Proctor, C. Kim, D. Neher, T.-Q. Nguyen, *Adv. Funct. Mater.* **2013**, *23*, 3584.
- [101] J. Vollbrecht, V. V. Brus, *Adv. Electron. Mater.* **2020**, *6*, 2000517.
- [102] M. Burgelman, P. Nollet, S. Degraeve, *Thin Solid Films* **2000**, *361*, 527.
- [103] M. Burgelman, K. Decock, S. Khelifi, A. Abass, *Thin Solid Films* **2013**, *535*, 296.
- [104] B. E. Pieters, K. Decock, M. Burgelman, R. Stangl, T. Kirchartz, in *Advanced Characterization Techniques for Thin Film Solar Cells*, Vol. 2 (Eds: D. Abou-Ras, T. Kirchartz, U. Rau), Wiley-VCH, Weinheim, Germany **2016**, Ch. 23.
- [105] T. Kirchartz, J. Nelson, *Top. Curr. Chem.* **2014**, *352*, 279.
- [106] N. Schopp, V. V. Brus, J. Lee, G. C. Bazan, T. Q. Nguyen, *Adv. Energy Mater.* **2020**, *11*, 2002760.
- [107] C. Kaiser, O. J. Sandberg, N. Zarrabi, W. Li, P. Meredith, A. Armin, *Nat. Commun.* **2021**, *12*, 3988.
- [108] A. M. Kay, O. J. Sandberg, N. Zarrabi, W. Li, S. Zeiske, C. Kaiser, P. Meredith, A. Armin, *Adv. Funct. Mater.* **2022**, *32*, 2113181.
- [109] G. Zhang, R. Xia, Z. Chen, J. Xiao, X. Zhao, S. Liu, H.-L. Yip, Y. Cao, *Adv. Energy Mater.* **2018**, *8*, 1801609.